INL/JOU-22-65784-Revision-0

A non-fueled nuclear-heated rod for in-pile transient boiling studies

December 2023

Changing the World's Energy Future

Connie M Hill, Charles P Folsom, Austin D Fleming, Robert J Armstrong, Nicolas E Woolstenhulme, Joshua David Fishler, John D. Bess, O. Richard Hernandez, Nicholas R. Brown, Colby B Jensen

INL is a U.S. Department of Energy National Laboratory operated by Battelle Energy Alliance, LLC

INL/JOU-22-65784-Revision-0

A non-fueled nuclear-heated rod for in-pile transient boiling studies

Connie M Hill, Charles P Folsom, Austin D Fleming, Robert J Armstrong, Nicolas E Woolstenhulme, Joshua David Fishler, John D. Bess, O. Richard Hernandez, Nicholas R. Brown, Colby B Jensen

December 2023

Idaho National Laboratory
Idaho Falls, Idaho 83415

http://www.inl.gov

Prepared for the
U.S. Department of Energy
Under DOE Idaho Operations Office
Contract DE-AC07-05ID14517

A Non-fueled Nuclear-heated Rod for In-pile Transient Boiling Studies

Connie M. Hill[a*], Charles P. Folsom[a], Austin D. Fleming[a], Robert J. Armstrong[a], Nicolas E. Woolstenhulme[a], Joshua D. Fishler[a] , John D. Bess[c], Richard Hernandez[b], Nicholas R. Brown[b], Colby B. Jensen[a]

a) Idaho National Laboratory, Idaho Falls, ID 83415, USA
b)University of Tennessee, Knoxville, Knoxville, TN 37996, USA
c) OECD Nuclear Energy Agency, Paris, France

*Corresponding author: connie.hill@inl.gov

Abstract

Separate-effects boiling experiments have recently been conducted in the Transient Reactor Test Facility at Idaho National Laboratory to investigate transient heating and irradiation effects on cladding-to-coolant heat transfer. Specifically, transient critical heat flux (CHF) remains an important area of research, and better understanding of this phenomenon has potential for improving predictive models related to operational and safety limits. Consequently, this knowledge is expected to improve efficiency of light-water reactor operations. A novel borated nuclear-heated rodlet (BNHR) was designed to enable observation of transient cladding-to-coolant heat transfer phenomena. The final BNHR design takes a surrogate approach, wherein nuclear heating is induced by $^{10}B(n, \alpha)$ reactions rather than derived from fissions in a fueled specimen. The structure of the BNHR consists of a hollowed out borated (B_{nat} ~2.05 wt. %) stainless steel tube with an hourglass-shaped outer surface, capped at both ends with non-borated stainless steel. This geometry allows for inner-rodlet instrumentation and generation of the highest nuclear heating rates near the center of the rodlet to ensure onset of boiling near instrumentation for real-time observation. A novel approach to measuring the nuclear energy deposition rate in the BNHR separate and apart from the influence of the coolant, termed the *n-α thermometer*, is also detailed in this paper. This device has demonstrated excellent repeatability, and measurements indicate predictive modeling results for energy deposition in the BNHR rod agree within a 10% margin of the experiment measurements. These results give confidence that the BNHR design has successfully met experiment objectives.

Keywords: Critical Heat Flux, TREAT, LWR, RISA

1. Introduction

Transient pool boiling critical heat flux (CHF) experiments have been conducted, recently, in the Transient Reactor Test Facility (TREAT) located at the Idaho National Laboratory (INL) (Folsom et al., forthcoming). The purpose of these in-pile transient boiling experiments in TREAT is to investigate cladding-to-coolant heat transfer phenomena in rapid nuclear heating conditions that might be experienced in light-water reactor (LWR) accident scenarios, such as during a reactivity initiated accident (RIA). A borated nuclear-heated rodlet (BNHR) has been specially designed for these initial experiments to investigate the effects of rapid surface heating and irradiation, such as radiation-induced surface activation (RISA) (Svanholm et al. 1995) on CHF predictions. These factors, among others, have been determined as highly important in the transient CHF phenomenon (Hernandez et al. 2020). Data acquired through these experiments are expected to illuminate heat transfer phenomena during, and as a result of, transient nuclear excursions. The knowledge gained is expected to better inform safety analysis for LWRs and contribute to significant improvement in plant operational efficiency.

One example of a way to improve safety analysis is to better quantify the heat transfer from the rod as it relates to departure-from-nucleate boiling (DNB), a condition wherein CHF is achieved and film boiling begins, during transient conditions. Prior research has indicated that the transient CHF can be significantly larger than what it would be during steady-state operating conditions. It follows that DNB can be delayed and affect heat transfer from the rod (Bessiron et al. 2007; Sugiyama et al. 2010). Consequently, the peak temperatures of fuel rods in some safety analysis scenarios, such as a RIA-induced boiling crises currently demarcated by predicted steady-

state condition CHF, are likely over predicted by a wide margin because DNB is not in reality achieved or delayed long enough to reduce the peak temperatures. It is also possible film boiling is not sustained long enough as a result of a short duration power pulse to cause detrimental heat build-up within the rods. Current fuel design thermal limits generally assume DNB predicted on a rod means a fail, which therefore may be unnecessarily limiting based on approved predictive relationships for DNB (NRC 2007). A better understanding, overall, of transient-induced boiling-water conditions to inform safety analysis predictive modeling is a primary goal of these experiments.

1.1 Overview of In-pile Boiling Experiment Design

The experiment in this study is housed in a capsule termed the Static-Environment Rodlet Transient Test Apparatus – Critical Heat Flux (SERTTA-CHF). The capsule is designed to provide a safe static water environment for testing in conditions that could lead to a substantial increase in vessel pressure due to the phase change of the heated water. The structural soundness of the containment structures as assessed through neutronics and thermal-hydraulics safety analysis are beyond the scope of this paper, which will focus on internal experiment components only. The first transient boiling phenomena experiments in TREAT are designated as SERTTA-CHF-A, CHF-B, and SERTTA-CHF-C.

TREAT not only provides the neutron irradiation necessary to simulate a transient nuclear excursion, but it also facilitates real-time, in-situ measurements provided by the strategic combination of dedicated instrumentation. The BNHR is key to the integration of neutron irradiation and supporting instrumentation for the successful illumination of transient cladding-to-coolant heat transfer phenomena for observation. The BNHR design and preliminary results are

the focus of this paper. More comprehensive descriptions of the SERTTA-CHF experiment are found elsewhere (Hernandez et al. 2019; Folsom et al., forthcoming).

The SERTTA-CHF design concept revolved around using specimen materials which would directly heat a LWR-diameter tube to CHF through nuclear interactions other than fission of actinide material. The reason for this novel separate-effects approach was to investigate specific transient CHF phenomena in a nuclear environment while removing many complicating factors present in typical LWR fuel. Such an approach was intended to help explore a phenomena space somewhere in between electrically heated and fission-heated transient tests. Like postulated-LWR events, these tests required prototypic ionizing radiation and the driving of rapid exponential heating rates of the specimen. Conversely, achieving transient CHF without typical fuel-in-cladding specimens would remove complicated pellet-cladding gap interactions and thermal transport in nuclear fuel, offer unique instrumentation opportunities, and minimize complex moderator effects upon specimen nuclear heating that may not be prototypic. The lack of fissile material in this approach was also noted for its value in facilitating logistics at non-radiological facilities and in reduction of test assembly costs.

Consideration for this non-fissile material, surrogate approach was given to several materials, informed by Monte Carlo neutronic predictions. Highly dense materials such as tungsten were considered as means for achieving transient CHF from prompt gamma heating and, while substantial in TREAT pulses, were predicted to produce inferior heating rates compared to strong neutron absorption reactions. Nuclear heating of gases bearing neutron absorbers, such as boron trifluoride (BF_3) or the isotope ^3He, was found to be very high, but engineering challenges with containment of an adequate mass of rapidly heated gas in a pressurized tube, in addition to challenges with modeling rapid heat transport from the gas into solid structure (tube wall), made

this option undesirable. The use of metallic alloys or ceramic materials bearing solid neutron absorbers was preferred for engineering reasons. Monte Carlo calculations showed that neutron-absorbing isotopes which deposit energy locally due to alpha particle recoil (i.e., ^{10}B or ^{6}Li) would likely deposit enough energy to achieve transient CHF. Boron-bearing ceramic pellets (B_4C, BN) were investigated and found to provide adequate heating as simulated fuel pellets but were ultimately not selected for the subject test matrix in order to simplify the thermal transport problem by avoiding pellet-to-cladding gap complications. Established borated alloys of stainless steel and aluminum, as well as a copper-lithium alloy, in the form of self-heated tubes were predicted to offer the best performance for test objectives. A boron-bearing alloy of austenitic stainless steel was ultimately selected due to high-temperature mechanical properties, chemical stability in water, and the ability to be machined and welded during specimen construction. The selected alloy was cast and formed into LWR-diameter rods by a commercial supplier specializing in research quantity lots of special alloys based on UNS S30467 (1.75-2.25 wt% B) per ASTM A887. The final material chosen has a boron content of 2.05 wt%.

Further Monte Carlo calculations were used to optimize the geometry of the BNHR. The ideal shape was determined to be a tube drilled from the aforementioned borated stainless steel rods. An outer surface “hourglass” shape with thicker tube walls on the ends was found to increase local neutron absorption self-shielding. This shape was employed so that the tube ends, which were otherwise predicted to experience power peaking, would exhibit a relatively depressed axial power profile based on heat conduction time constants in relation to rim thickness. The selected hourglass shape was predicted to facilitate CHF near the axial center of the rodlet where instrumentation is located for critical time-dependent measurements of transient heat transfer phenomena and to avoid end effects on heat transfer behavior. End caps constructed of non-borated

stainless steel were welded to the tube ends to maintain a dry environment inside the borated hourglass-shaped tube and to also aid in directing energy from the heater ends axially away from the heater rod surfaces.

An advanced design feature was considered that included axial boron content gradients in the BNHR that could be fabricated using 3D printing techniques. No shaping of the outer surface of the rodlet (graded wall thickness) would then be necessary. Scoping studies showed that this application would be successful in driving initial DNB at the center of the rodlet. However, this design approach was not implemented in the SERTTA-CHF experiments to date, primarily for non-technical reasons, but the hourglass design described above was selected for use with a total heated length of 102 mm and a diameter of 9.5 mm, which tapers to 7.3 mm at the axial center.

1.2 Experiment Instrumentation

The instrumentation package for the SERTTA-CHF experiments consists of type K thermocouples (TCs), optical-fiber based pyrometers, a custom designed electro-impedance boiling detector, and the ^{10}B(n, α) Thermometer, an instrument designed for in-situ measurement of rodlet nuclear heating termed the *n-α thermometer* for short. The combination of all of these instruments allows for revealing, real-time observation of nuclear transient CHF phenomena during the experiment. A more detailed description of these instruments can be found elsewhere (Folsom et al., forthcoming; Jensen et al. 2017). Figure 1 illustrates the general orientation of instrumentation relative the BNHR and highlights some features and positioning of the *n-α thermometer* and the pyrometers.

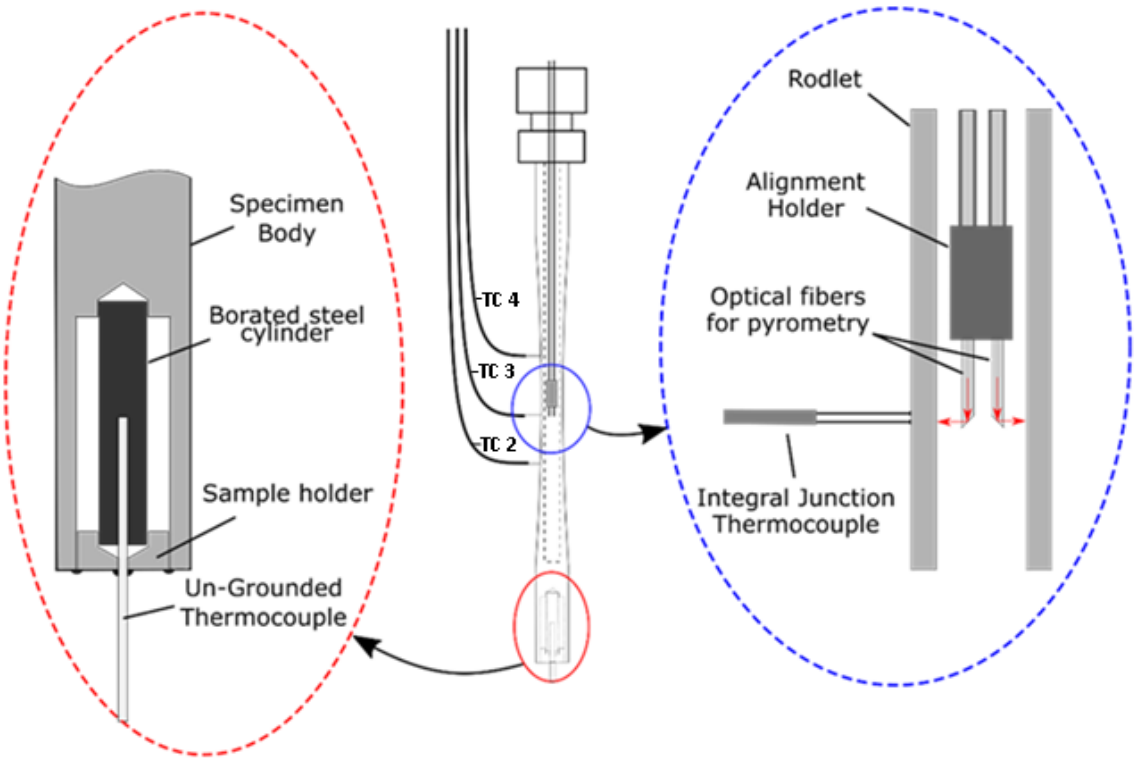

Figure 1. Diagram of the hourglass design for the boron nuclear-heated rodlet (center) and the associated instrumentation (right and left). The *n-α thermometer* is shown in detail on the left.

Four type K TCs are welded to the outer cladding surface of the BNHR to investigate axial surface temperature of the borated segment of the rodlet. Figure 2 shows the placement of the TCs, approximately 2 cm apart, along the hourglass-shaped rodlet in one of the final stages of experiment assembly. Two TCs are placed near the coil heater that controls water temperature pre-irradiation, and one TC is dedicated to water temperature measurement apart from all other experiment components. Two optical-fiber-based pyrometers are placed inside the BNHR to measure inner surface temperature at the axial center of the rodlet. The pyrometers provide a non-contact method of measuring the temperature inside of the BNHR. The lower end of instrument measurement range is 300°C with limited time response. For these experiments, the functional range is greater than 600°C, and the pyrometers serve as an independent measurement of the

cladding outside of the water environment. Figure 1 also shows how the pyrometers are placed in relation the BNHR and other instrumentation.

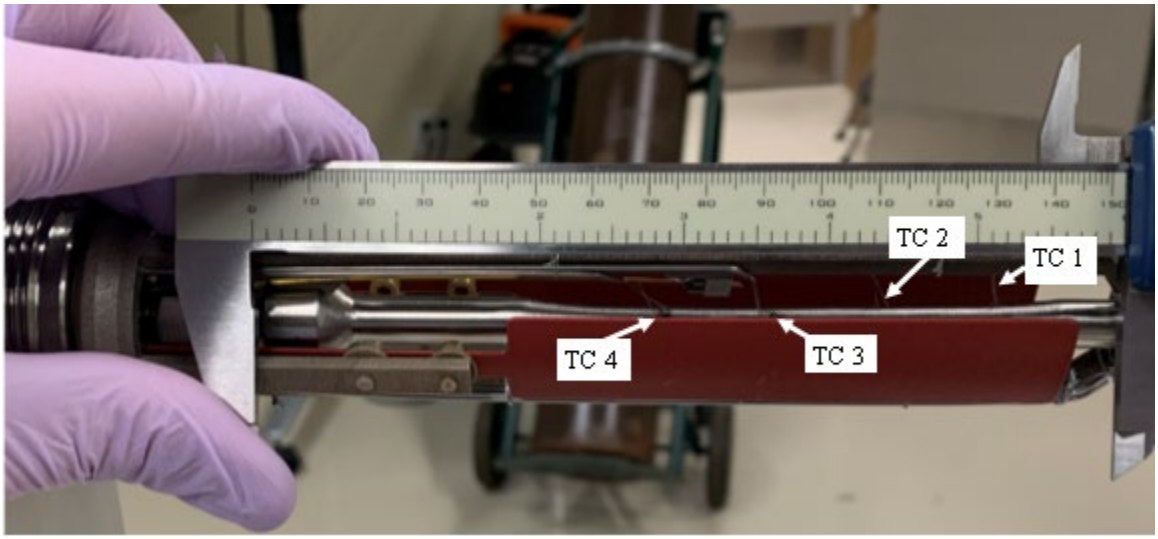

Figure 2. SERTTA-CHF BNHR and surrounding instrumentation in one of the final stages of assembly for the SERTTA-CHF-A irradiation in TREAT. The caliper shows TCs welded to the surface of the rodlet, approximately 2 cm apart.

The electro-impedance boiling detector, developed at INL, measures change of capacitance between two conducting plates surrounding the BNHR due to water voiding during the experiment (Jensen et al. 2017). These measurements provide some indication of nuclear transient-induced thermo-hydraulic water conditions. Figure 2 also shows how the boiling detector plates (colored red) are aligned with the BNHR.

A small design revision was made after the SERTTA-CHF-A irradiation capsule was built to include a neutron thermometer, termed the *n-α thermometer*, to provide a more direct online measure of energy deposited in the borated stainless steel. The design of the *n-α thermometer* utilized a type K TC, embedded within the same borated steel material as used in the heater section of the rodlet. This assembly was placed in a hollow cavity located in the non-borated bottom cap of the BNHR with an insulative gas volume surrounding it to minimize heat loss to a controlled

behavior. This novel approach allows for real-time, in-situ measurement of nuclear heating, or energy deposition, within the BNHR separate and apart from the influence of fluctuating water conditions during the test. See Figure 1 for a diagram of this device and its location relative to the BNHR.

2. Methods

Extensive use of predictive neutronics and thermal-hydraulics analysis combined with engineering judgment led to a maturity in the BNHR design that indicated CHF could be achieved, and DNB would be initiated at the desired location along the rodlet in a TREAT experiment. Final neutronics analysis that includes calculations of nuclear heat generation rates (HGRs) using a finer mesh of the chosen material and geometry for the BNHR is presented here with some thermal-hydraulics analysis to aid in verifying BNHR performance. Analysis supporting the design of the *n-α thermometer* is also presented.

2.1 BNHR Nuclear Heating Predictive Neutronics and Thermal-hydraulics Analysis

Nuclear HGRs were predicted for a mature BNHR design concept using Monte Carlo N-particle (MCNP) code, version 6.1 (Goorly et al. 2013) with ENDF/B-VII.1 nuclear data cross sections (Chadwick et al. 2011). See Figure 3 for MCNP plots illustrating a horizontal and vertical mid-section view of the modeled experiment in the SERTTA-CHF capsule for TREAT irradiation simulation. Nuclear HGRs were calculated for all cells in a fine mesh representing the borated segment of the rodlet using MCNP F6:n and F6:p combined energy deposition tallies. The thin central region of the rodlet was divided into four concentric right-cylindrical tubes with equal radial thickness. Axially, these tubes were divided into 10 segments of equal length. The upper and lower ends of the borated segment of the rodlet (end caps excluded) that had curvature on the

outer surface added six additional concentric right-cylindrical tubes of equal radial thickness. These tubes were also divided into 10 axial segments, however, with different lengths corresponding to the outer surface curvature of these segments. See Figure 4 for an illustration of the applied mesh. The mesh configuration shown in this figure for the upper end of the rodlet is mirrored at the bottom end of the rodlet.

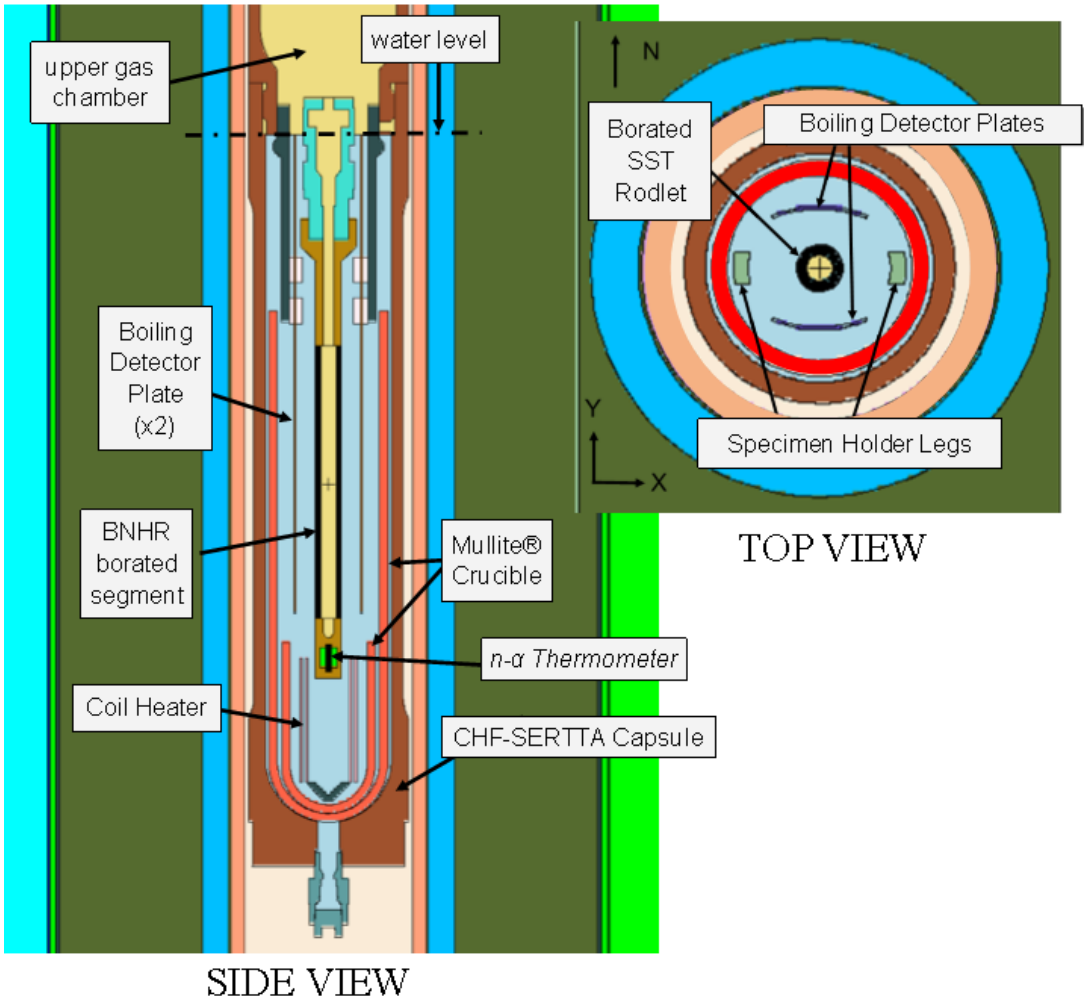

Figure 3. MCNP plots depicting the SERTTA-CHF experiments in TREAT.

The mesh is defined by 10 radial segments and 30 axial segments. Some of the cells include water that immediately surrounds the rodlet within the outermost cylindrical boundary of the mesh.

The analysis results presented here are calculated from a model representing a 4.2 %Δk/k reactivity step insertion core configuration (transient rods removed from the core) with the experiment starting at room temperature. The model was processed in eigenvalue mode at 2,500,000 particles per cycle for 220 cycles, skipping 20 cycles to achieve less than 3% relative error in the individual mesh cells. Calculated nuclear HGRs serve as input for follow-on thermal analysis.

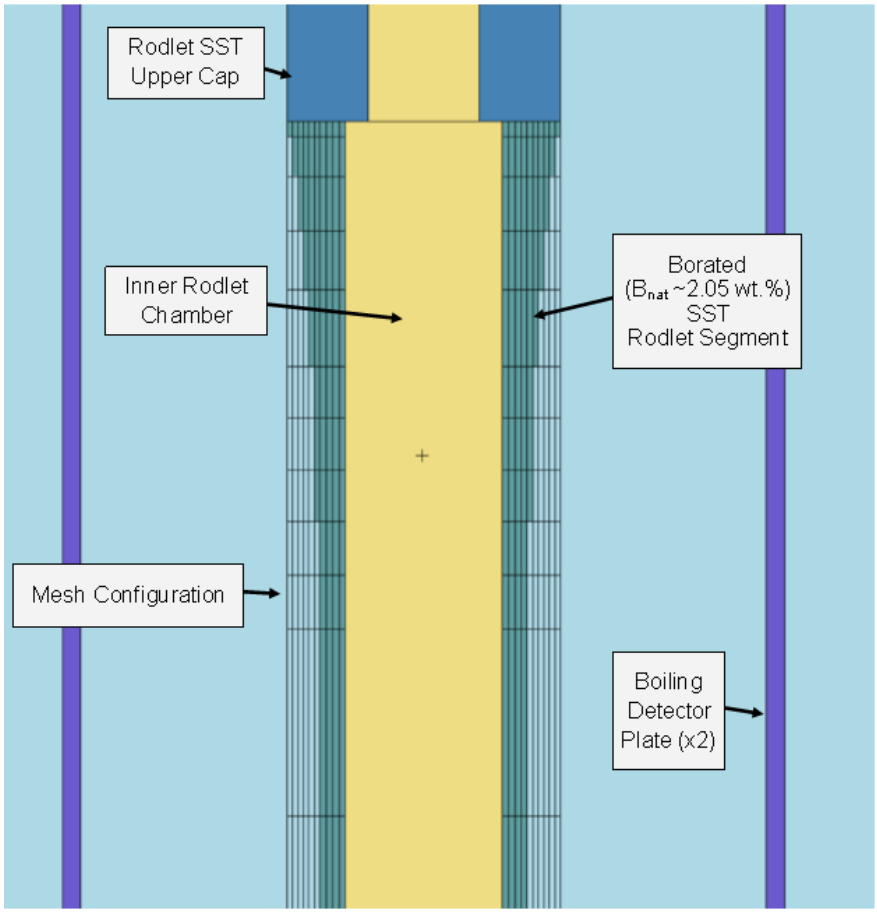

Figure 4. MCNP plot illustrating the mesh configuration used in analysis for the BNHR tube with hourglass-shaped outer surface geometry.

2.2 $^{10}B(n,\alpha)$ Thermometer Design

The *n-α thermometer*, as illustrated in Figure 1, has a borated stainless steel (2.05 wt% B_{nat}) cylinder piece with a type K TC located in the center of it. A cavity in the rodlet bottom is machined such that the borated component is only held in place at the ends with minimal surface contact area to reduce heat loss from the specimen. The borated component will experience neutron heating which is directly measured by the type K TC without the high heat losses to the surrounding water, as experienced by the BNHR rod. The nuclear energy deposited in the specimen can be determined by measuring the temperature and knowing the material properties and total mass of the specimen.

Locating the *n-α thermometer* in the bottom of the rodlet is ideal because of the similar water temperature and neutronic conditions. Specifically, this location benefits from similar neutron moderation from the water in the experiment as in the main section of the rodlet, and the surrounding water is expected to be at the same temperature. The *n-alpha specimen* is in close enough proximity to the rodlet tube such that it should experience the same potential time-dependent variations in the flux due to control rod motion in the TREAT core (Klotzkin et al. 1984); however, the location of this piece in relation to the BNHR rodlet will see a slightly different flux (and consequently nuclear heating rate) due to the axial location and being centered at a focal point in what can be considered a flux trap created by the moderating water surrounding a cylinder. However, this difference should be minor and a potential bias correction has been identified by MCNP simulation.

For correct operation of the *n-α thermometer*, the gas gap around the borated steel cylinder needs to be maintained. In particular, it cannot allow water in from the surrounding environment. This is achieved by performing two welds, one between the TC sheath and the sample holder (weld #1) and another between the sample holder and specimen body (weld #2), identified in Figure 5. These welds were performed using a micro-tig welder, qualified on prototype materials and tested

using helium leak detection. The assembly of the device began with a dry fit of the components, shown in Figure 5. Once in place, the weld between the TC and the sample holder is conducted. The TC and sample holder are then removed from the rodlet, and a helium leak check is performed to ensure this weld has sealed the TC to the sample holder. Next the assembly is replaced, the weld between the sample holder and specimen body is made, and a detailed inspection of the weld is performed.

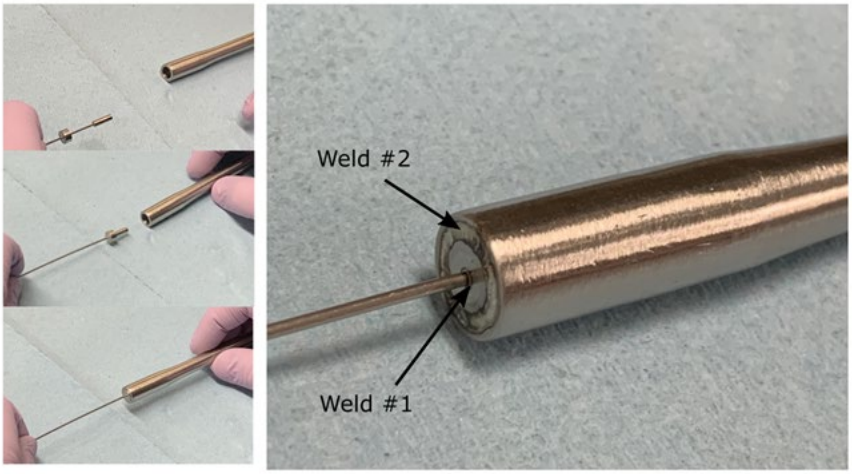

Figure 5. Assembly of the *n-α thermometer* for SERTTA-CHF experiments.

Neutronics analysis was also conducted on the *n-α thermometer* to estimate nuclear HGRs. The applied mesh, see Figure 8, was a division into four radially equal segments beyond the radius of the TC insert. HGR results for these cells were then used in thermal-hydraulics analysis to estimate the temperature profile of the *n-α thermometer* for the duration of the transient. Comparison of the predicted temperature profile and the measured temperature profile in TREAT is expected to reveal the level of agreement between nuclear HGR predictions and experiment measurements to inform predictive neutronics modeling.

3. Results and Discussion

3.1 BNHR Nuclear HGRs

The predicted nuclear HGR results for the mesh cells of the BNHR and surrounding water modeled in MCNP are presented in Table 1. The thin, straight segment of the tube has an average nuclear HGR of ~0.39 W/g-MW on the outer surface. The units represent the power generated per gram of specimen within the mesh cells per MW core power. Cells at the outer rim of the rodlet have the highest nuclear HGRs, as expected, with some peaking on the upper and lower ends. Prior scoping studies showed a depression in axial power at the rodlet ends; however, these studies were done without a radially segmented mesh. The resultant peaking at the ends in this final analysis prompted additional thermal analysis to address concerns of DNB instantiation at the ends rather than at the center of the rodlet. Such a scenario would prove detrimental to the thermal-hydraulic performance of the BNHR. Ideally, the BNHR will experience the highest radial heat flux to the coolant at the axial center where the instruments are located with the purpose of avoiding end effects in heat transfer behavior. This will ensure that initiation of boiling occurs where the instruments are present to monitor the changing thermal-hydraulic conditions and resulting BNHR temperatures as a function of time for heat transfer analysis.

A 2D axisymmetric finite element model of the BNHR with the non-borated material welded on the ends was developed to verify that initiation of boiling would not start at the ends of the BNHR where the nuclear HGRs are the highest. The 2D mesh of the BNHR created in Abaqus (Smith et al. 2009) is shown in Figure 6. The model assumes pure conduction through the system including the volumes representing fluids which is only approximately valid during very short times but assumed appropriate to evaluate relevant heat transfer of concern. Spatial distribution of

internal heat generation representative of those calculated using the MCNP model is crucial to capture the radial and axial heat transfer at the center and ends of the BNHR. The Abaqus subroutine DFLUX was paired with the model shown in Figure 7b to distribute the heat generation rate appropriately. The heat loads were combined with a Gaussian-shaped pulse typical of a reactivity step insertion transient in TREAT (Woolstenhulme et al. 2018; Woolstenhulme et al. 2020).

Table 1. MCNP-calculated nuclear HGRs for the borated nuclear-heated rodlet (BHNR) and surrounding water mesh cells.

Nuclear HGRs [W/g-MW]										
Mesh Row	Rodlet Mesh Column (Initial Experiment Temperature 20°C)									
	1	2	3	4	5	6	7	8	9	10
1	0.366	0.362	0.356	0.355	0.371	0.380	0.359	0.395	0.427	0.474
2	0.263	0.237	0.244	0.257	0.258	0.282	0.309	0.343	0.395	0.041
3	0.242	0.227	0.220	0.235	0.243	0.279	0.320	0.385	0.044	0.045
4	0.222	0.230	0.232	0.222	0.272	0.314	0.382	0.045	0.043	0.043
5	0.229	0.231	0.226	0.229	0.311	0.355	0.043	0.044	0.044	0.042
6	0.256	0.263	0.271	0.301	0.357	0.046	0.043	0.043	0.042	0.044
7	0.245	0.267	0.278	0.312	0.354	0.043	0.043	0.043	0.041	0.041
8	0.269	0.274	0.295	0.328	0.403	0.043	0.041	0.042	0.041	0.041
9	0.294	0.290	0.327	0.381	0.043	0.044	0.042	0.041	0.041	0.039
10	0.286	0.292	0.310	0.374	0.043	0.043	0.043	0.042	0.042	0.039
11	0.304	0.294	0.328	0.386	0.042	0.040	0.041	0.042	0.041	0.042
12	0.309	0.307	0.327	0.390	0.041	0.041	0.041	0.040	0.040	0.040
13	0.294	0.292	0.325	0.387	0.042	0.042	0.042	0.043	0.042	0.042
14	0.294	0.304	0.340	0.404	0.043	0.043	0.042	0.043	0.042	0.042
15	0.305	0.322	0.336	0.400	0.043	0.043	0.042	0.041	0.042	0.041
16	0.309	0.297	0.322	0.371	0.041	0.041	0.040	0.040	0.040	0.041
17	0.305	0.309	0.331	0.393	0.042	0.041	0.042	0.042	0.042	0.041
18	0.290	0.311	0.345	0.401	0.042	0.043	0.045	0.044	0.043	0.043
19	0.293	0.318	0.347	0.391	0.041	0.043	0.043	0.043	0.042	0.042
20	0.270	0.312	0.331	0.397	0.043	0.043	0.043	0.041	0.042	0.042
21	0.290	0.288	0.324	0.377	0.045	0.043	0.044	0.044	0.043	0.042
22	0.293	0.285	0.315	0.381	0.043	0.045	0.044	0.041	0.041	0.040
23	0.270	0.278	0.295	0.335	0.391	0.043	0.045	0.042	0.041	0.044
24	0.268	0.275	0.292	0.324	0.388	0.044	0.047	0.045	0.044	0.044
25	0.270	0.275	0.287	0.313	0.365	0.047	0.046	0.045	0.045	0.045
26	0.250	0.241	0.254	0.275	0.320	0.375	0.045	0.045	0.043	0.042
27	0.231	0.231	0.229	0.251	0.280	0.319	0.380	0.041	0.042	0.042
28	0.242	0.242	0.234	0.241	0.240	0.276	0.320	0.371	0.044	0.042
29	0.261	0.236	0.241	0.248	0.284	0.289	0.300	0.343	0.416	0.044
30	0.362	0.237	0.342	0.356	0.360	0.364	0.395	0.395	0.402	0.488

The resulting axial and radial heat flux were calculated in the BNHR through the transient. Radial and axial heat flux profiles during the transient at 0.1 and 0.223 seconds are shown in Figure 7 (the time of peak power in the Gaussian pulse was 0.2 seconds). These results show that the axial

conduction at the ends of the rod into the non-borated stainless steel end caps helps to lower the radial heat flux into the water at these locations, even though the predicted nuclear HGRs are highest at the ends (Table 1). This provides confidence that end peaking on the BNHR, as it relates to heat transfer from the rodlet to the water, will not occur, and that initiation of film boiling and subsequent rapid temperature increase of the rodlet occurring away from the center where the TCs and pyrometers are focused will be avoided.

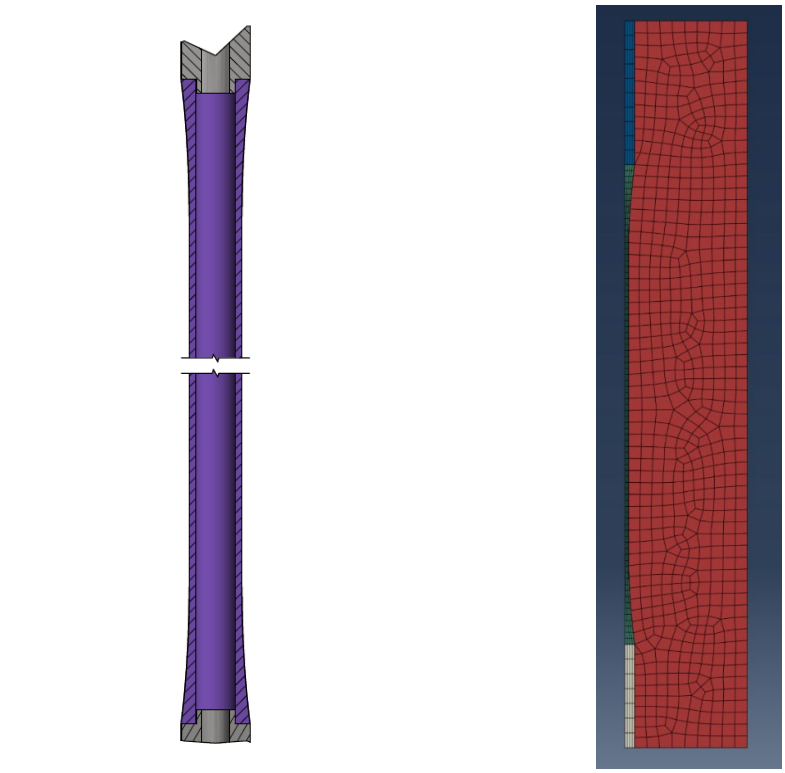

Figure 6. a) Cross-section view of the BNHR (purple) with welded on SS304 top and bottom end caps and b) Abaqus 2D axisymmetric model representing the BNHR (green) with SS-304 end caps (gray and blue) and water (red).

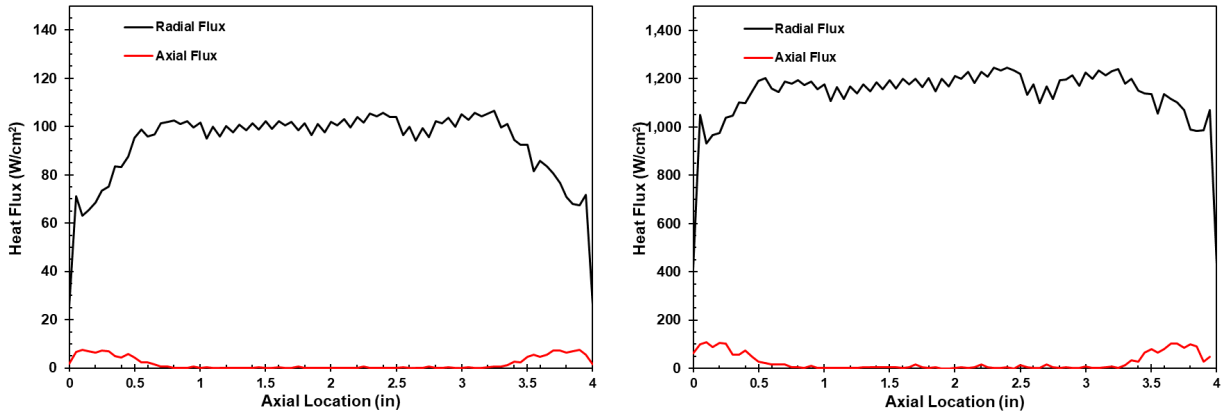

0.1 seconds 0.223 seconds (time of maximum flux)

Figure 7. Radial and axial heat flux (absolute value) calculations along length of BNHR from Abaqus simulation (0 corresponds to bottom of rod).

3.2 $^{10}B(n,\alpha)$ Thermometer

Neutronics analysis for the *n-α thermometer* was also conducted with MCNP. No mesh divisions were made axially; however, the cylinder of borated steel was divided into five radial segments: The central segment just above the TC insert ~0.08 mm in diameter and four surrounding annuli of ~0.296 mm in thickness. The outer radius of the modeled cylindrical specimen is 4.26 mm. The mesh division is illustrated in Figure 8. Table 2 shows the layer results that are used in subsequent thermal analysis to predict a thermal response to the applied transient. Note that the outer rim average is 0.426 W/g-MW. This is approximately 8.4 % higher than the average outer rim surface HGRs calculated for the rodlet.

Table 2. *$^{10}B(n, \alpha)$ specimen* mesh HGR results.

Borated Cylinder Segment	**HGR [W/g-MW]**
Outer Annulus	0.426
Annulus 1	0.366
Annulus 2	0.358
Annulus 3	0.363
Inner Annulus	0.309

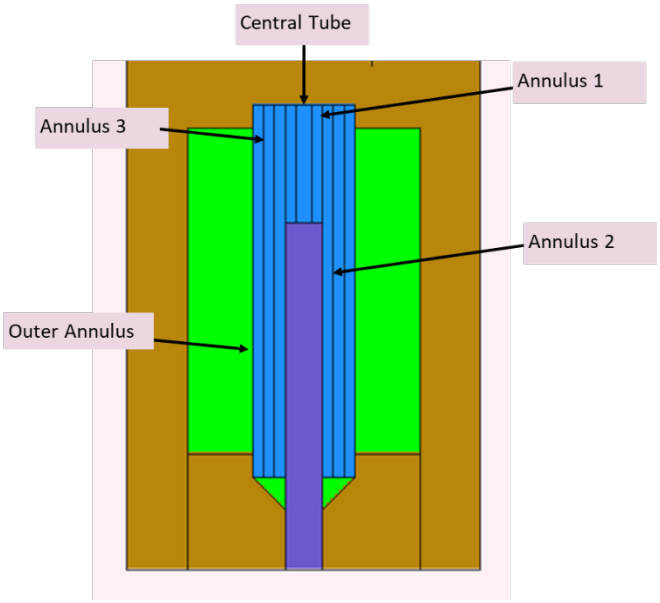

Figure 8. MCNP plot illustrating mesh scheme for $^{10}B(n, \alpha)$ *thermometer* HGR analysis.

The nuclear HGRs of the *n-α specimen* from the MCNP results were applied to a detailed 3-D Abaqus model to validate the nuclear HGR estimates of the borated stainless steel material in the BNHR and *n-α thermometer* through comparison to temperature measurements during the experiment. The same geometry of the *n-α thermometer* shown in Figure 8 was created in Abaqus with a detailed model of the TC in the *n-α thermometer* verified via x-ray radiography. See Figure 9. The nuclear HGRs shown in Table 2 were applied with the same discretization method as used in MCNP. Appropriate gap interactions were applied between the borated stainless steel component and the TC as well as to the surrounding stainless-steel material that makes up the lower end cap of the BNHR.

Like the other SERTTA-CHF capsules, the SERTTA-CHF-B capsule was run through multiple transient irradiations. In this case, five transients were executed with a 4.2% Δk/k reactivity step insertion in TREAT, and the control rods were re-inserted precisely to limit the

transient to 1800 MJ of core energy release. This type of transient results in a Gaussian-like power pulse with a full-width-at-half-max (FWHM) pulse width of 109 milliseconds. The transient irradiations were repeated five times on the SERTTA-CHF-B capsule with all conditions being the same except the fifth transient, which was performed with approximately 20°C more subcooling. Figure 10a shows the five TREAT power transients and integrated energy curves. The repeatability of TREAT is evident with these transients. Figure 10b shows the resulting temperatures measured in the *n-α thermometer*, excluding data from the fifth transient because of the different starting temperature. The *n-α thermometer* demonstrated excellent repeatability in these results.

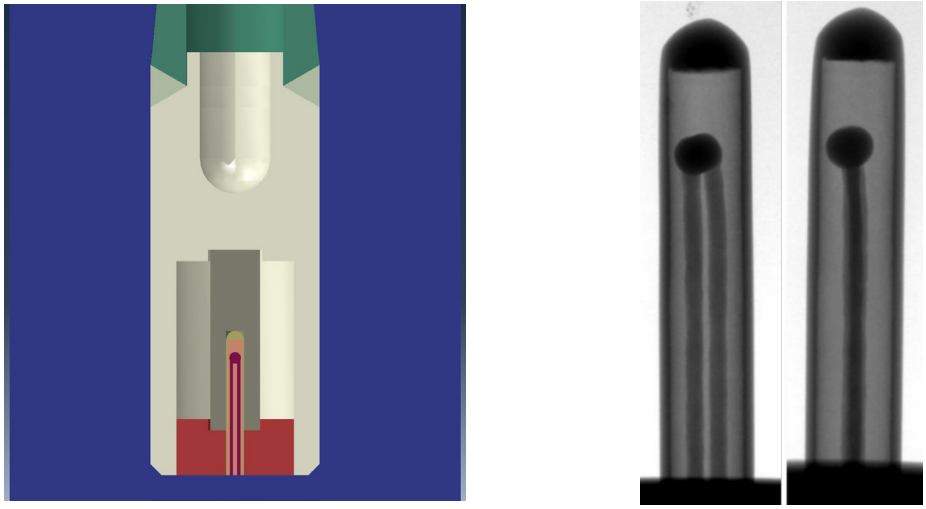

a) **b)**

Figure 9. a) Abaqus model of the *n-α thermometer* (shown in dark gray) with the detailed TC wires and junction created from b) an x-ray radiograph of the TC.

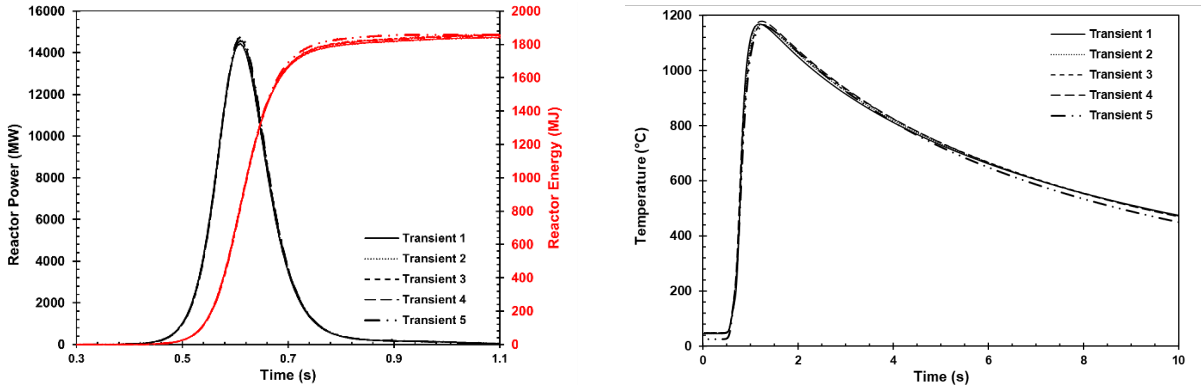

a) **b)**

Figure 10. TREAT experimental data depicting SERTTA-CHF-B irradiations and corresponding core energy release (left) and corresponding BNHR (n, α) thermometer temperature readings (right).

The measured TREAT power data from SERTTA-CHF-B was used in the Abaqus model of the *n-α thermometer*. The peak temperature in the TC junction of the Abaqus model was compared to the peak temperature of the *n-α thermometer* results during the experiment. The results displayed in Figure 11a show the nominal nuclear HGRs as well as a factor of 1.097 applied to the HGRs. A 9.7% increase in the predicted HGRs showed excellent agreement with the peak temperatures measured during the experiment. The rate of cooling between the *n-stainless-steel* and the experiment shows some variation but that is due to the gap interaction modeled between the borated stainless steel cylinder and the stainless steel end cap for the *n-α thermometer* as well as thermal-hydraulic conditions on the outside of the BNHR; due to the time scales and the gas gap design insulating the borated stainless steel cylinder, however, these factors have very little influence on the peak temperatures seen during the simulations.

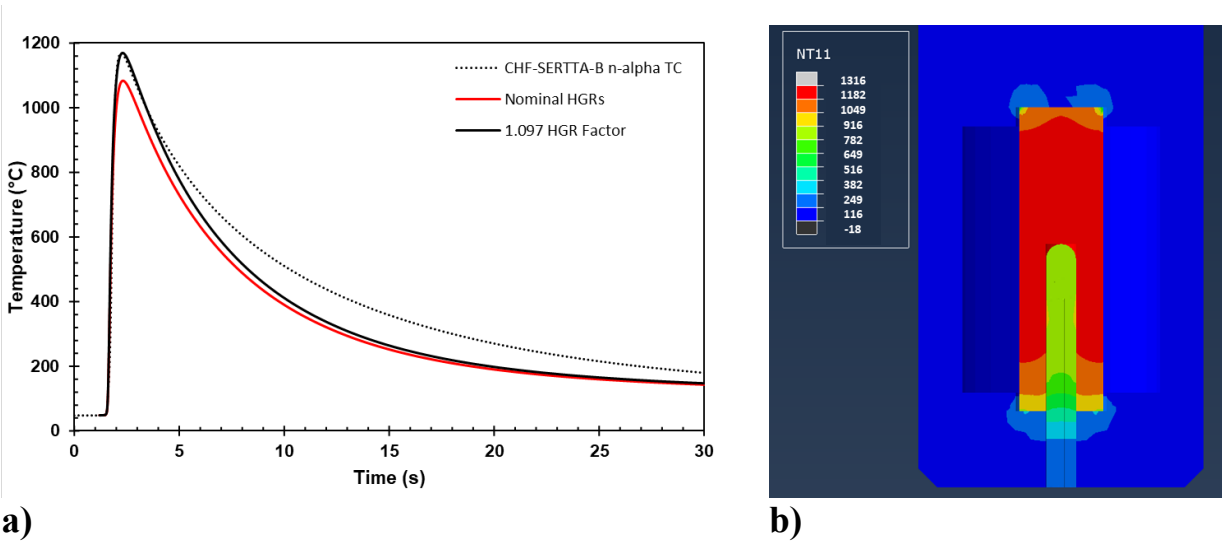

a) **b)**

Figure 11. a) Temperature history of the n-α thermometer Abaqus predictions compared to the experiment results for various factors on the HGRs and b) temperature (°C) contour plot at the time of peak temperature in the n-α thermometer.

Figure 11b shows a temperature contour plot at the time of peak temperature in the *n-α thermometer*. The uniform axial temperature gradient in the borated stainless-steel material around the TC tip confirms very little axial heat loss occurs, and the material behaves adiabatically near the TC during the very short time it takes to reach the peak temperatures. The repeatability of the experiment results and agreement of measured vs. predicted values within 10% gives high confidence that the n-α thermometer is capable of capturing the nuclear heating energy deposition into the rodlet as a function of time. This demonstrates significant value towards achieving experiment objectives regarding observation of cladding-to-coolant heat transfer.

3.3 TREAT Experiment Results

Temperature measurements from Transient-1 in the series of SERTTA-CHF-A irradiations, acquired by TCs placed along the rodlet, are presented in Figure 12. Data from TC 1 was not retrievable; however, the TC closest to center of the rodlet and those approximately 2 cm

apart on each side did provide sufficient data for observation. This power pulse achieved a peak power of approximately 5.63 GW which is rather low compared to 14.4 GW power peak experienced in the SERTTA-CHF-B irradiations. Note that peak temperatures on either side of the central TC are approximately 100°C less than that for the central TC. These results indicate that heating of the rodlet is significantly higher in the central axial region for the duration of the experiment.

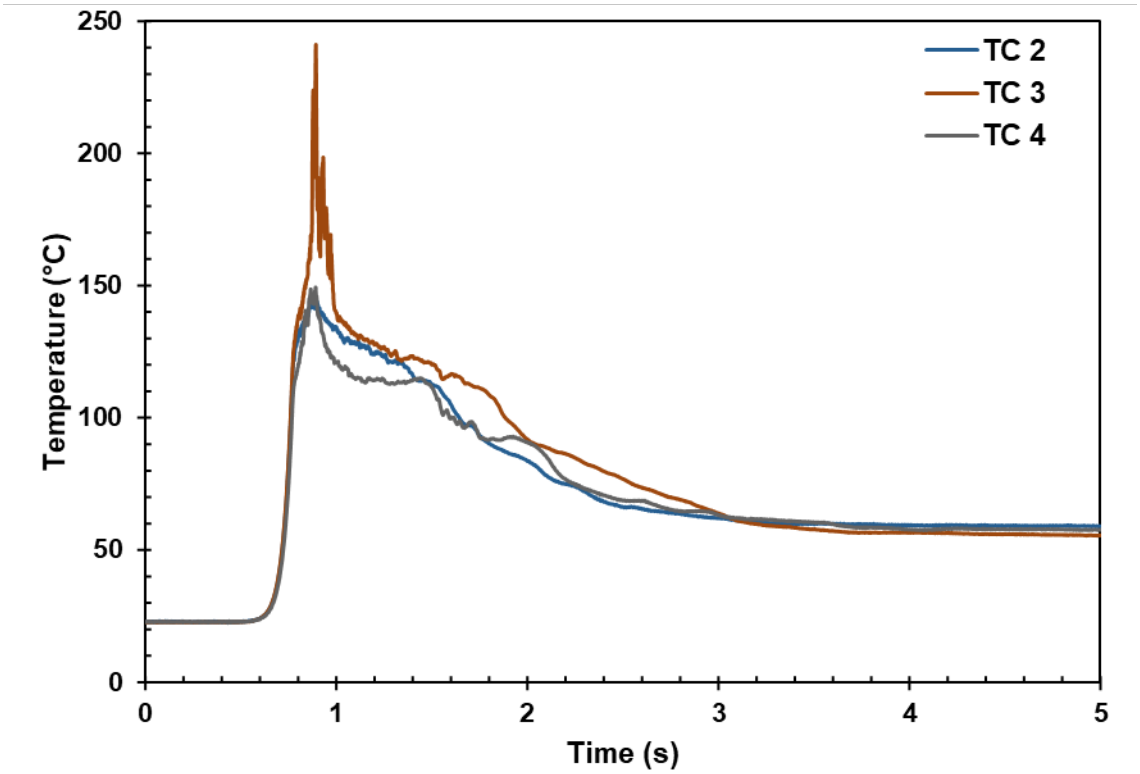

Figure 12. Rodlet TC temperature measurements for Transient 1 of the SERTTA-CHF-A series of irradiations in TREAT.

Temperature measurements for the duration of Transient-1 in the SERTTA-CHF-B series of irradiations, of the water (water TC), inner BNHR wall (Pyro A and Pyro B), outer BNHR wall at axial center (Rodlet TC1), and of the isolated nuclear heat generation within the borated material that makes up the rodlet (n-α TC) are observed together in Figure 13. The applied TREAT narrow pulse that peaks at ~ 14.4 GW is overlaid on the same temperature graph to illustrate the response

of the various independent instruments relative to the timing of the pulse. The most immediate response is from the TC attached to the outer BNHR wall, likely due to its configuration of an integral junction with the measured surface and the thermo-elements compared to the sheathed TC used in the *n-α thermometer*. Both TCs display a similar heating and cooling pattern; however, peak temperatures differ by about 282°C. This offset is largely due to the significant and rapid heat removal from the BHNR by the water. The oscillations in the curve for Rodlet TC1 show the influence of nucleate and film boiling turbulence from bubble and film movement on the TC measurements as the oscillations are more prominent in the early stages of developing film boiling than they are during the few seconds of cooling time displayed. The pyrometer measurements show a similar pattern of temperature increase and decrease when compared to TC measurements from n-α TC and Rodlet TC1. The Pyro A and B temperatures fall somewhat under the n-α TC results. Lower peak temperatures as measured by the pyrometers are expected, due to the difference (~8.4% lower) in the MCNP-calculated nuclear HGRs and the cooling influence of the water on the BNHR tube walls as opposed to the conditions at the location of the n-alpha TC.

Rodlet TC1 measurements show a steep decline in temperature at about 6.5 seconds when the rodlet rewets. These measurements soon reach equilibrium with water TC measurements; whereas, the n-alpha TC continues a slower and steadier decline in temperature. This rate of decline in the n-alpha TC temperature measurements is expected given the limited means of heat transfer from the *n-α thermometer*. All of these measurements contribute essential information for the overall experiment and indicate excellent performance of the SERTTA-CHF experiments and the quality of the resulting data.

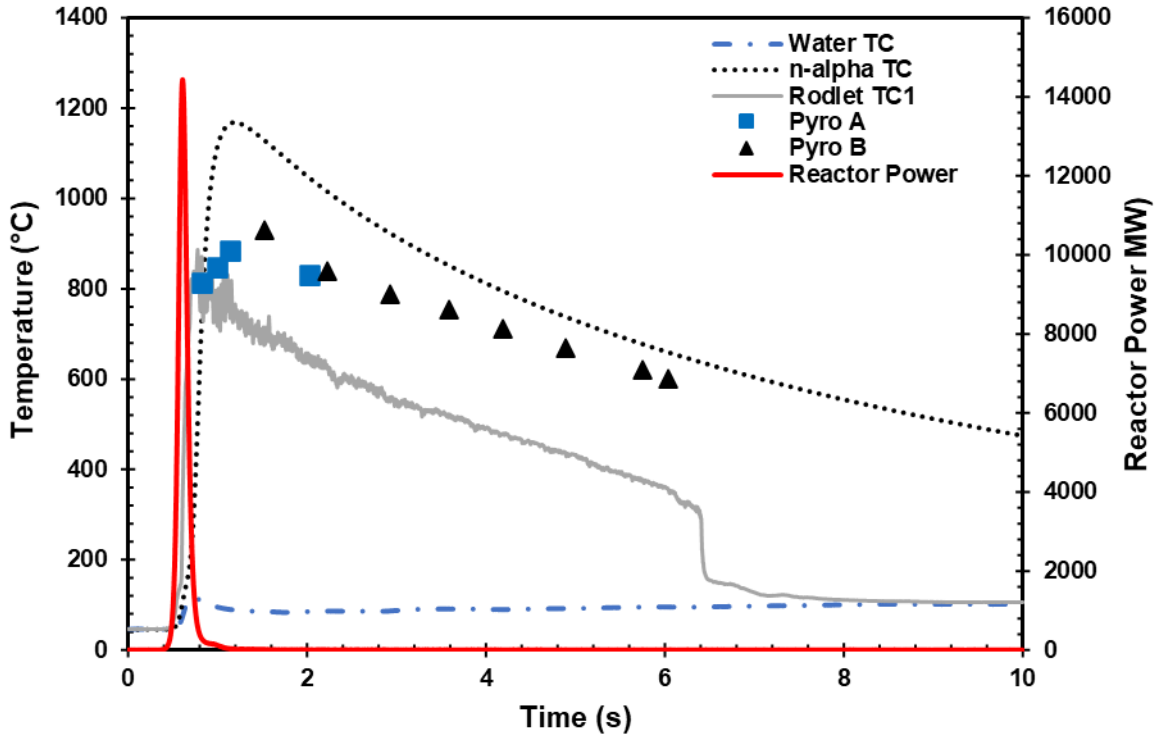

Figure 13. CHF SERTTA-B Transient 1 results (boiling detector not included).

4. Summary & Conclusions

The design of the BNHR in SERTTA-CHF experiments in TREAT has successfully achieved the objective to convert an applied transient neutron pulse into sufficient heat along a rodlet with near prototypic LWR fuel diameter to create boiling conditions in a water environment that allow for observation of transient CHF phenomena. Neutronics and thermal-hydraulics analysis, substantiated by TREAT experiment results, showed that the hourglass-shaped outer surface worked to drive an initial boiling condition leading to CHF and DNB at the desired central location of the rodlet where instrumentation could take time critical readings for meaningful comparison.

TCs placed directly on the surface of the rodlet and surrounded by water have shown to be inadequate for measuring direct nuclear heat generation within the rodlet because of competing heat transfer mechanisms. This problem was solved by the design of the *n-α thermometer*, integrated into the bottom cap of the rodlet. This additional *n-α thermometer* design proved excellent repeatability along with TREAT transient power measurements. The *n-α thermometer* temperature measurements and thermal predictions predicated on nuclear HGR estimates demonstrated a level of agreement, within 10%, that would indicate nuclear heating in the rodlet can be measured separate and apart from the influence of the surrounding water. Knowledge of initial energy deposition into the BNHR is vital in obtaining meaningful conclusions regarding heat transfer to the coolant. These results also increase confidence that DNB was initially achieved near the center of the rodlet as models indicated. These results also allow for quantification of water-cooling impact on the rodlet. All measurements from these experiments will be carefully analyzed more comprehensively and reported in future work. The *n-α thermometer* design has potential value for many other experiments in the TREAT facility, and the SERTTA-CHF design can provide continued insight into in-pile boiling behaviors.

5. Acknowledgements

The authors acknowledge the many contributions from an expansive team: Todd Pavey and Devin Imholte for experiment design and integration, Leigh Ann Astle for project management and integration, Ashley Lambson, Kevin Tsai, Eric Larsen for fabrication and experiment diagnostics, Robert Armstrong and Ben Chase for analysis, Sterling Morrill, Gary Owens, John Carter, James Parry, J.R. Biggs, Anthony Maestas, and many others for TREAT operations, John Wagner, Steve Hayes, and Daniel Wachs for support, guidance, and advice.

This research made use of the resources of the High Performance Computing Center at Idaho National Laboratory (INL), which is supported by the Office of Nuclear Energy of the U.S. Department of Energy (DOE) and the Nuclear Science User Facilities under Contract No. DE-AC07-05ID14517.

This work was supported through the INL Laboratory Directed Research & Development Program under DOE Idaho Operations Office Contract DE-AC07-05ID14517. Accordingly, the U.S. Government retains and the publisher, by accepting the article for publication, acknowledges that the U.S. Government retains a nonexclusive, paid-up, irrevocable, worldwide license to publish or reproduce the published form of this manuscript, or allow others to do so, for U.S. Government purposes.

6. References

Bess, J.D., Woolstenhulme, N.E., Jensen, C.B., Parry, J.R., and Hill, C.M. 2019. "Nuclear characterization of a general-purpose instrumentation and materials testing location in TREAT." Annals of Nuclear Energy, 124, 270–294. https://doi.org/10.1016/j.anucene.2018.10.011.

Bessiron, V. 2007. "Modelling of Clad-to-Coolant Heat Transfer for RIA Applications." Journal of Nuclear Science and Technology 44(2): 211–221. https://doi.org/10.1080/18811248.2007.9711275.

Bessiron, V., Sugiyama, T.,Fuketa, T. 2007. "Clad-to-Coolant Heat Transfer in NSRR Experiments." Journal of Nuclear Science and Technology 44(5): 723–742. https://doi.org/10.1080/18811248.2007.9711861.

Folsom, C.P., Armstrong, R.J., Woolstenhulme, N.E., Fleming, A.D., Hill, C.M., Jensen, C.B., and Wachs, D.M. Forthcoming. "Design of Separate-Effects In Pile Transient Boiling Experiments at the TREAT Facility." Nuclear Engineering and Design.

Goorley, Goorley, J.T., James, M.R., Booth, T.E., Brown, F.B., Bull, J.S., Cox, L.J., Durkee, Jr., J.W., Elson, J.S., Fensin, M.L., Forster, III, R.A., Hendricks, J.S., Hughes, III, H.G., Johns, R.C., Kiedrowski, B.C., Martz, R.L., Mashnik, S.G., McKinney, G.W., Pelowitz, D.B., Prael, R.E., Sweezy, J.E., Waters, L.S., Wilcox, T., and Zukaitis, A.J. 2013. "Initial MCNP6 Release Overview-MCNP6, Version 1.0." LA-UR-13-22934, Los Alamos National Laboratory. https://doi.org/10.2172/1086758.

Chadwick, M.B., Herman, M., Oblozinsky, P., Dunn, M.E., Danon, Y., Kahler, A.C., Smith, D.L., Pritychenko, B., Arbanas, G., Archilla, R., Brewer, R., Brown, D.A., Capote, R., Carlson, A.D., Cho, Y.S., Derrien, H., Guber, K., Hale, G.M., Hoblit, S. , Holloway, S., Johnson, T.D., Kawano, T., Kiedrowski, B.C., Kim, H., Kunieda, S., Larson, N.M., Leal, L. Lestone, J.P., Little, R.C., McCutchan, E.A., MacFarlane, R.E., Macinnes, M. Mattoon, C.M., McKnight, R.D., Mughabghab, S.F., Nobre, G.P.A., Palmiotti, G. Palumbo, A., Pigni, M.T., Pronyaev, V.G., Sayer, R.O., Sonzogni, A.A., Summers, N.C., Talou, P., Thompson, I.J., Trkov, A., Vogt, R.L., van der Marck, S.C., Wallner, A., White, M.C., Wiarda, D., and Young, P.G. 2011. "ENDF/B-VII.1 Nuclear Data for Science and Technology: Cross Sections, Covariances, Fission Product Yields and Decay Data." Nuclear Data Sheets 112(12): 2887–2996. https://doi.org/10.1016/j.nds.2011.11.002.

Hernandez, R., Folsom, C.P., Woolstenhulme, N.E., Jensen, C.B., Bess, J.D., Gorton, J.P., Brown, N.R. 2020. "Review of pool boiling critical heat flux (CHF) and heater rod design for CHF experiments in TREAT." Progress in Nuclear Energy 123: 103303. https://doi.org/10.1016/j.pnucene.2020.103303.

Jensen, C. 2017. "FY17 Report for Instrumentation Development for the Transient Testing Program." INL/EXT-17-43444-Rev000, Idaho National Laboratory. https://doi.org/10/2172/1473628.

Klotzkin, G., Swanson, R.W., Hart, P., Harrison, L.J. 1984. Time Dependence of Test Fuel Power Coupling During Transient Reactor Test Facility Irradiation Experiments. Nuclear Science and Engineering, 86:2, 206–218. https://doi.org/10.13182/NSE84-2

Okrent, D., Dickerman, C.E., Gasidlo, J., O'Shea, D.M., and Schoeberle, D.F. 1960. "THE REACTOR KINETICS OF THE TRANSIENT REACTOR TEST FACILITY (TREAT)." ANL-6174, Argonne National Laboratory. https://doi.org/10.2172/4117807.

Smith, M. 2009. "ABAQUS/Standard User's Manual, Version 6.9." Dassault Systèmes Simulia Corp. Providence, RI.

Svanholm, K., Breghi, M.P., D'Auria, F, Ianiri, R. 1995. "Halden reactors IFA-511.2 and IFA-54x: experimental series under adverse core cooling conditions." Experimental Thermal and Fluid Science 11(1): 77–100. https://doi.org/10.1016/0894-1777(94)00138-x.

U.S. Nuclear Regulatory Commission (NRC). 2007. "Standard Review Plan: Fuel System Design." NUREG-0800, 4.2, Rev.3, U.S. Nuclear Regulatory Commission. https://www.nrc.gov/docs/ML0707/ML070740002.pdf.

Woolstenhulme, N., Baker, C., Bess, J., Chapman, D., Dempsey, D., Hill, C., Jensen, C., and Snow, S. 2018. *New Capabilities for In-Pile Separate Effects Tests in TREAT*. in *Transactions of the American Nuclear Society Summer Meeting 2018*. Philadelphia, PA.

Woolstenhulme, N., Baker, C., Jensen, C.B., Chapman, D.B., Imholt, D.D., Oldham, N., Hill, C.M., and Snow, S.D. 2019. "Development of Irradiation Test Devices for Transient Testing." Nuclear Technology 205(10): 1251–1265. https://doi.org/10.1080/00295450.2019.1590072.

Woolstenhulme, N., Fleming, A., Holschuh, T., Jensen, C., Kamerman, D., and Wachs, D. 2020. "Core-to-specimen energy coupling results of the first modern fueled experiments in TREAT." Annals of Nuclear Energy 140: 107117. https://doi.org/10.1016/j.anucene.2019.107117.